AD-763 781

ANALYSIS OF THE MECHANICS OF PERFORATION OF PROJECTILES IN METALLIC PLATES

J. Awerbuch, et al

Technion-Israel Institute of Technology

AD 763 781

Prepared for:

Air Force Office of Scientific Research

May 1973

DISTRIBUTED BY:

NTIS

National Technical Information Service
U. S. DEPARTMENT OF COMMERCE
5285 Port Royal Road, Springfield Va. 22151

Security Classification

DOCUMENT CONTROL DATA - R & D

(Security classification of title, body of abstract and indexing annotation must be entered when the overall report is classified)

1. ORIGINATING ACTIVITY (Corporate author)
TECHNION RESEARCH AND DEVELOPMENT FOUNDATION
HAIFA, ISRAEL

2a. REPORT SECURITY CLASSIFICATION
UNCLASSIFIED

2b. GROUP

3. REPORT TITLE
ANALYSIS OF THE MECHANICS OF PERFORATION OF PROJECTILES IN METALLIC PLATES

4. DESCRIPTIVE NOTES (Type of report and inclusive dates)
Scientific Interim

5. AUTHOR(S) (First name, middle initial, last name)
J AWERBUCH S R BODNER

6. REPORT DATE
May 1973

7a. TOTAL NO. OF PAGES
~~34~~ 38

7b. NO. OF REFS
19

8a. CONTRACT OR GRANT NO.
F44620-72-C-0004

b. PROJECT NO.
9782-02

c. 61102F

d. 681307

9a. ORIGINATOR'S REPORT NUMBER(S)
MED Rpt No.40
Sci Rpt No.3

9b. OTHER REPORT NO(S) (Any other numbers that may be assigned this report)
AFOSR - TR - 73 - 1150

10. DISTRIBUTION STATEMENT
Approved for public release; distribution unlimited.

11. SUPPLEMENTARY NOTES
TECH, OTHER

12. SPONSORING MILITARY ACTIVITY
AF Office of Scientific Research (NAM)
1400 Wilson Blvd.
Arlington, Va. 22209

13. ABSTRACT
A mathematical model has been developed to describe the mechanism of normal perforation of projectiles in metallic targets. The perforation process is considered to be divided into three interconnected stages. The analysis accounts for an effective mass of the bullet due to part of the target material moving with the bullet, the deformation of the bullet during penetration, and the increase strength of the target material at high rates of loading. The analysis enables the residual velocity to be calculated as a function of the target thickness and its mechanical and physical properties, and of the mass, geometry and impact velocity of the projectiles. The geometry of the cavity, i.e. entrance and exit diameters and plug thickness, are factors in the analysis and are empirical quantities. The present theory can also predict the force-time curve and the contact time for the perforation process.

DD FORM 1 NOV 65 1473

UNCLASSIFIED
Security Classification

Security Classification

14. KEY WORDS	LINK A ROLE	LINK A WT	LINK B ROLE	LINK B WT	LINK C ROLE	LINK C WT
BALLISTICS, TERMINAL						
PERFORATION						
PENETRATION						
ARMOR						
IMPACT						
DYNAMIC PLASTICITY						
PUNCHING						

UNCLASSIFIED

Security Classification

CONTRACT F 44620-72-C-0004 MAY 1973

SCIENTIFIC REPORT NO. 3

ANALYSIS OF THE MECHANICS OF PERFORATION OF PROJECTILES IN METALLIC PLATES

by

J. Awerbuch and S.R. Bodner

MED REPORT NO. 40

Material Mechanics Laboratory

Department of Materials Engineering

Technion - Israel Institute of Technology

Haifa, Israel

Approved for public release;
distribution unlimited.

The research reported in this document has been supported in part by the AIR FORCE OFFICE OF SCIENTIFIC RESEARCH under Contract F 44620-72-C-0004, through the European Office of Aerospace Research, (EOAR), United States Air Force.

IC

i.D

Analysis of the Mechanics of Perforation of Projectiles in Metallic Plates

by

J. Awerbuch[1] and S.R. Bodner[2]

Abstract

A mathematical model has been developed to describe the mechanism of normal perforation of projectiles in metallic targets. The perforation process is considered to be divided into three interconnected stages. The analysis accounts for an effective mass of the bullet due to part of the target material moving with the bullet, the deformation of the bullet during penetration, and the increased strength of the target material at high rates of loading. The analysis enables the residual velocity to be calculated as a function of the target thickness and its mechanical and physical properties, and of the mass, geometry and impact velocity of the projectile. The geometry of the cavity, i.e. entrance and exit diameters and plug thickness, are factors in the analysis and are empirical quantities. The present theory can also predict the force-time curve and the contact time for the perforation process.

---

[1]Lecturer, Department of Materials Engineering, Technion - Israel Institute of Technology.

[2]Professor, Department of Materials Engineering, Technion - Israel Institute of Technology.

Notation

A - projection of nose of projectile on the target plate

A_1 - cross sectional area of the cavity in the first stage

A_2 - cross sectional area of the cavity in the second stage

A_p - cylindrical surface area of plug

b - plug length

D_1 - diameter of the cavity in the first stage of the perforation process (considered equal to entrance diameter)

D_2 - diameter of the cavity in the second stage of the perforation process (diameter of plug)

D_3 - exit diameter

e - radial width of shear zone of the target plate

F - resultant force on effective mass of projectile

F_i - inertial force

F_c - compressive force

F_s - shearing force

F_1, F_2, F_3 - total forces acting on the combined projectile and effective added mass during the different stages of the perforation process

F_{i2}, F_{c2}, F_{s2} - inertial, compressive and shearing forces acting on the projectile during the second stage

h - thickness of target plate

K - numerical constant depending on the shape of the projectile nose

m - instantaneous mass of projectile

m_o - original mass of projectile

Notation (cont'd)

m_1 - projectile's mass at the end of the first stage

m_2 - projectile's mass at the end of the second stage

t - time

t_1, t_2, t_3 - duration times for the different stages of perforation

t_f - total time for the perforation process

V - instantaneous velocity

V_i - impact velocity

V_f - final velocity

V_1, V_2, V_3 - projectile's velocity during the different stages of the perforation process

$\bar{V}_2$ - velocity at end of second stage

$\bar{V}_3$ - velocity at end of third stage, equal to V_f

x - penetration depth of the projectile and effective added mass

α - semi apex of conical nose of projectile

γ_f - dynamic ultimate shear strain

$\dot{\gamma}$ - shear strain rate

ρ - density of target material

μ - coefficient of viscosity for shearing deformation

σ_c - dynamic ultimate compressive stress

τ - dynamic ultimate shear stress

ξ - displacement of combined projectile and plug during third stage

Introduction

Perforation of a target plate due to the impact of a projectile may occur by a number of mechanisms such as petal formation (or dishing), ductile hole enlargement, plug formation, and the fragmentation (scabbing) of the target material (as shown schematically by Goldsmith [1]). Various theories have been proposed to explain the resistance of metallic plates to projectile penetration. Due to the complexity of the problem, the suggested analytical models are generally simplified by some basic assumptions and approximations.

The two main approaches that have been used to analyze this problem are those of energy balance and of conservation of momentum. The energy balance method was applied by Taylor [2] who studied the enlargement of a circular hole by a conical head projectile perforating a thin plate and derived an expression for the total work required for plastic deformation. Thomson [3], also using the energy method, derived equations for the energy dissipation due to plastic deformation, heating, and inertial resistance of the target material. A similar approach was proposed by Brown [4] to evaluate the energy dissipated during the process of bullet containment in thin plates.

A different approach for the case of perforation of thin plates was proposed by Zaid & Paul [5,6]. Their method is based on momentum balance for the target-projectile system which requires that the terminal shape of the perforated plate be specified. A similar procedure was used by Nishiwaki [7] who proposed a theory for the perforation of thick plates based upon data derived from static tests.

Investigations on plug formation during perforation were made, among

others, by Recht & Ipson [8] who dealt with the case of high velocity impact. Recht & Ipson [8] developed an energy analysis for the case of the plug mode of failure from which the residual velocity could be calculated provided the minimum perforation velocity is known.

Most proposed analyses are restricted to the case of high velocity impact in order to justify a number of assumptions such as a constant velocity during the perforation of thin plates, the absence of plastic deformation beyond the immediate zone surrounding the hole, and a constant pressure on the projectile. These analyses are also restricted to the case for which the projectile is not deformed during the perforation process and are generally based upon only one of the possible mechanisms of perforation. Actual perforation of a target plate, however, may occur by a combination of two or more mechanisms. For example, the thickness of the sheared plug is generally smaller than the target thickness and the plugging process commences only after the projectile is embedded some distance in the target plate. For this reason an approach based on a single deformation mechanism would not be applicable for the case of projectile impact at ordnance velocities. In fact, the residual velocities derived from those theories based on a single mechanism are generally higher than the experimental results, e.g. [9].

The present investigation is an analysis of the perforation process considering various deformation mechanisms to be acting at different stages of the process. In this manner the various types of deformations could be considered in an overall manner and the analysis would be more representative of the actual circumstances. A preliminary study of this nature was performed by Awerbuch [10] and expanded upon by Goldsmith and Finnigan [11]. The

present paper is a further development of those investigations and resolves a number of limitations. The perforation process is considered to consist of three interconnected stages. The present analysis enables fairly accurate predictions of post perforation velocities, contact times, and force-time histories. The analysis still relies on a few empirical quantities which can be determined from a small number of tests. Once these are determined for a given projectile and target material, predictions can be obtained over a wide range of projectile velocities and target thicknesses.

Reproduced from best available copy.

Preliminary Discussion

A relatively simple model to describe the mechanism of penetration and perforation of projectiles in metallic plates was presented in an earlier paper [10]. In that formulation, the perforation process was divided into two stages. The first was the compressive stage in which the forces acting on the projectile were an inertial force and a compressive force, and the second stage was that of plug formation and ejection.

The inertial force in the first stage is due to the acceleration of the mass of the target material in contact with the projectile in the direction of motion. The expression for this force component is obtained by equating the work done by the inertial force acting on the projectile to the change of kinetic energy of the displaced target material. The compressive force also acting on the projectile is due to the compressive strength of the target material in contact with the projectile. Another basic assumption for this stage is that mass from the target material is added to the projectile during the penetration process.

The second and final stage, according to the preliminary analysis, starts when the ejected plug is set into motion as a rigid body. In this stage, the inertial force and the compressive force do not act on the projectile and the mass of the projectile does not change. The only force, therefore, during this stage is that due to the shearing of the ejected plug from the target plate which was assumed to be constant.

Final velocities of projectiles computed according to this preliminary

model were compared to experimental final velocities and reasonably good agreement was obtained when the mechanical strength properties were raised in an arbitrary manner to account for the high rate of straining. The comparison was carried out for the case of 0.22 inch caliber lead bullet having a muzzle velocity of 400 m/sec and target plates of commercially pure aluminum, aluminum alloy, and mild steel of 1-6 mm thickness.

The results of an extensive series of ballistic experiments have been reported by Goldsmith and Finnigan [11]. Hard steel spheres of 0.125 to 0.5 inch diameter impacted and perforated 0.05 to 0.25 inch thick 2024 aluminum and SAE 1020 and 4130 steel alloy plates at impact velocities of 500 to 8800 ft/sec. Comparisons were made of the experimental final velocities to those calculated on the basis of the preliminary model [10] and to a slightly modified form of it developed in [11]. The principal modification was that the shearing force in the second stage of the perforation process was taken to be proport l to the length of the plug still in contact with the target plate r r than a constant. Comparison of the final velocity obtained with this modification to that obtained experimentally showed slightly better agreement.

The experimental results of [11] and those of an extensive experimental program recently conducted [15] have indicated that the preliminary model developed in [10] is incomplete on some important points. These are:

(1) The final velocities of projectile computed from the model are not in good agreement with experimental final velocities for the cases of high velocity projectiles and for perforation of thick plates.

(2) The preliminary model does not predict an important experimental observation, namely, that the difference between the initial and final velocities decreases for initial velocities slightly greater than the ballistic limit.

(3) The force-time curve obtained from this model is not fully realistic.

In order to overcome these limitations of the preliminary model, a more detailed analysis has been developed in which the perforation process was considered to consist of three separate but interconnected stages. The observations and results of an extensive experimental program served to motivate certain assumptions of the analysis. Those experimental results and comparisons with predictions based on the present analysis are presented in an associated paper [15].

Analysis

One principal mechanism of the plate perforation process is plug formation and ejection. When the thickness of the sheared plug, b, is equal to zero, there is no punching and the mechanism of failure is considered to be the ductile type. When the plug's thickness is equal to the thickness of the target plate, h, perforation is completely by plug formation. However, the mechanism of perforation is usually a combination of the two processes with a transition stage between them. The ratio of the plug to plate thicknesses b/h depends primarily on the mechanical and physical properties of the projectile and target materials.

In the first stage of penetration, Fig. 1a, shearing does not occur so this stage is identical to that described in the preliminary analysis [10]. The only forces acting on the projectile are the inertial force and the compressive force.

The second stage of penetration, Fig. 1b, is the onset of shearing of a plug from the target plate. In this stage of incipient plugging, three forces are considered to act on the projectile: an inertial force and a compressive force (as formulated in the first stage), and a shearing force. The shearing force is due to the motion relative to the target plate of target material which is accelerated by the projectile during this stage. The change of the effective mass of the projectile, due to the addition of target material moving with it, is considered in this stage as well as in the first stage This stage ends when the plug is completely joined to the projectile and both are moving at the same velocity, Fig. 1c.

The third stage, Fig. 1d, starts when the ejected plug and the projectile are moving together as a rigid body. The only force during this stage is the shearing force which acts on the plug's circumference and along its whole length. The viscous nature of this shearing force at high rates of straining is considered.

Since the time of contact between the projectile and the target is very short (the time duration is about 10-30 μsec for the case of a 0.22 inch caliber lead bullet moving at a velocity of 400 m/sec), the heat generated at the projectile - target plate interface does not dissipate. A very thin film of liquid is produced between the projectile and the target plate. The coefficient of friction between the two bodies is therefore very small so the frictional forces can be neglected. This conclusion has been made by Krafft [12] and by other investigators.

The equation of motion for the perforation process in the direction of motion is

$$\frac{d}{dt}(mV) = -F \qquad (1)$$

where F is the resultant force acting on the projectile, m is the instantaneous mass of the projectile, and V is the instantaneous velocity of the projectile in the medium.

In general, the force F is the resultant of three main components; F_i the inertial force of the target material, F_c the compressive force, and F_s the shearing force. Therefore,

$$\frac{d}{d\tau}(mV) = -(F_i+F_c+F_s) \qquad (2)$$

The particle velocity due to elastic stress wave propagation in the target is neglected in this analysis. This particle velocity, for example, would be of the order of 1 m/sec for a 0.22 inch caliber lead bullet moving at a velocity of 400 m/sec, e.g. Davies [13]. The effect of the propagation of the plastic stress wave is also neglected since it can be assumed that its velocity would be smaller than the velocity of the projectile for most target materials.

The projectile therefore transmits kinetic energy only to the mass it displaces. It is assumed that the element of mass of the target material in contact with the projectile is set into motion while the remainder of the target material remains at rest. Each mass element is considered to move normal to the surface of the nose of the projectile. This is possible on the basis that the target material is compressible.

Another related assumption is that the effective mass of the projectile increases during the penetration process due to addition of the target material displaced in the direction of motion. Part of the kinetic energy imparted to the added mass by the projectile remains stored in the combined effective mass of the projectile while the remainder is converted to plastic deformation and heat.

In the first stage of the penetration process, only the inertial and compressive forces are considered to act on the projectile. The inertial force is not distributed uniformly on the projectile's nose surface

but depends on the shape of the nose. Equating the work done by the reaction of the inertial force on the target material to the change of the kinetic energy of the displaced material (neglecting the work done in changing the volume of a mass element due to its compressibility) leads to

$$dF_{in}dx_n = \frac{1}{2}\, dmV_n^{\,2} \tag{3}$$

where dF_{in} is the normal inertial force acting on an element area dA_n of the projectile, dx_n is the displacement of a mass element of the target material normal to the projectile surface, and V_n is the velocity of a mass element in a direction normal to the projectile surface.

According to the above assumptions, the mass element dm of the target material of density ρ which is displaced by the projectile as it advances dx_n would be

$$dm = \rho dx_n dA_n \tag{4}$$

Substituting Eq. (4) into Eq. (3) leads to

$$dF_{in} = \frac{1}{2}\, \rho(dA_n)V_n^{\,2} \tag{5}$$

F_i can be determined for each projectile's shape by integrating the component of dF_{in} in the direction of motion over the surface of the projectile.

As an example, for a cylindrical projectile with a flat end:

$$V_n = V, \quad \int_S dF_{in} = F_i, \quad \text{and} \quad \int_S dA_n = A$$

so that

$$F_i = \frac{1}{2} \rho A V^2 \tag{6}$$

If the geometry of the projectile's nose is more complicated, then:

$$F_i = \frac{1}{2} K \rho A V^2 \tag{7}$$

where K is a numerical constant depending on the geometry. Values of K obtained by integration for some typical geometries are given in Table I:

TABLE I

Nose Shape	K
Flat	1
Sphere	1/2
Cone (semi apex angle α)	$\sin^2\alpha$

The compressive force is distributed uniformly in the direction of motion on the projectile's nose surface and can be expressed as $F_c = \sigma_c A$.

A is the projected area of the projectile's nose on the target plate and σ_c is the ultimate compressive strength of the target plate at the applied straining rate. The equation of motion for the first stage, Eq. (2), could therefore be written as follows:

$$\frac{d}{dt}(mV) = V\frac{dm}{dt} + m\frac{dV}{dt} = F_1 = -\frac{1}{2}K\rho A_1 V^2 - \sigma_c A_1 \qquad (8)$$

where the projected area A_1 includes the effect of possible flattening of the projectile's nose. A_1 is taken to be constant during stage 1 and is measured by the entrance opening. In the actual physical process, A_1 would be a function of x since the projectile deforms with penetration distance. This effect can be considered in an overall average manner to within the level of accuracy of this analysis.

The inertial force F_i and compressive force F_c are considered to act on the effective mass of the projectile which includes the target material displaced by the projectile and moving with it (Fig. 1a). The problem of physically locating the added mass with respect to the projectile is not readily resolved since compressibility effects would have a large influence. However, this determination is not required for the purpose of the present analysis. It is important to note that the measure of the penetration depth of the projectile, x, is that of the combined mass and not that of the original projectile by itself. That is, the value of x is the distance from the initial impact surface to the front of the target material that is moving at the projectile velocity (Fig. 1a). The effective mass of the

combined projectile for use in the equation of motion is therefore $m_o+\rho A_1 x$ where m_o is the original mass of the projectile.

The rate of change of the effective mass of the projectile would be

$$\frac{dm}{dt} = \rho A_1 \frac{dx}{dt} = \rho A_1 V \tag{9}$$

Substituting Eq. (9) and the relation

$$\frac{dV}{dt} = \frac{dV}{dx}\frac{dx}{dt} = V\frac{dV}{dx}$$

into Eq. (8) leads to:

$$\rho A_1 V^2 + (m_o+\rho A_1 x)\, V \frac{dV}{dx} = -\frac{1}{2} K\rho A_1 V^2 - \sigma_c A_1 \tag{10}$$

Equation (10) can be solved by separation of variables to give

$$V_1(x) = \left\{\left[V_1^2+\frac{\sigma_c}{\rho(1+0.5K)}\right]\left(\frac{m_o/\rho A_1}{m_o/\rho A_1+x}\right)^{2+K} - \frac{\sigma_c}{\rho(1+0.5K)}\right\}^{1/2} \tag{11}$$

where $V_1(x)$ is the velocity of the combined projectile and added mass.

The time for the combined projectile to penetrate a distance x can be calculated by numerical integration of the expression

$$= \int_0^x \frac{1}{V_1(x)}\,dx = \int_0^x \left\{\left[V_1^2+\frac{\sigma_c}{\rho(1+0.5K)}\right]\left(\frac{m_o/\rho A_1}{m_o/\rho A_1+x}\right)^{2+K} - \frac{\sigma_c}{\rho(1+0.5K)}\right\}^{-1/2} dx \tag{12}$$

The force-time curve for the first stage of penetration can be obtained from Eqs. (8), (11) and (12). The first stage ends when $x=h-b$ ($t=t_1$) and the process of shearing starts. The value of the plug thickness b, which is an essential factor for the determination of the various quantities at the end of the first stage, can only be obtained empirically at the present state of development of the analysis. It is shown in [15] that the ratio b/h is essentially constant for a given projectile and target material within the range of ordnance velocities.

In the second stage of incipient plugging, the inertial force continues to act on the projectile and can be expressed as

$$F_{i2} = \frac{1}{2} K\rho A_2 V^2$$

where A_2 is the cross sectional area of the cavity in the second stage. This area can, in general, be considered a function of x, $A_2 = A_2(x)$, in the force expressions and in the equations of motion. The experimental results indicate that for most cases A_2 is close to A_1 so that the complete cavity can be considered to be cylindrical. In some cases there is appreciable enlargement, i.e. the exit diameter is much larger than the entrance diameter. The diameter can then be considered to vary linearly with x from D_1 at $x=h-b$ to D_3 at $x=h$ to give a quadratic function for $A_2(x)$. The following development of the equations of motion will be restricted to constant A_2. In the subsequent comparisons with experiments, [15], A_1 and A_2 were taken to be equal and the average of the entering and exit areas. Check studies taking $A_1=A_1(x)$ and $A_2=A_2(x)$ showed little difference in the final

Reproduced from best available copy.

results.

The shape constant K in the inertial force expression was set equal to 0.5 for the second stage since for standard ordnance projectiles (not armour piercing) the projectile's nose deforms and tends toward a spherical shape. This result can be seen from ballistic photographs as well as from the geometry of the ejected plugs and the deformed projectiles. This change of K would imply an artificial discontinuity in the force. In practice, the discontinuity is very small and not observed unless the time increments in the computational procedure are taken to be very small.

The compressive force also acts during the second stage of penetration and its initial value would be $F_c = \sigma_c A_2$. The second stage ends when the mass element at the rear side of the target plate moves at the same velocity of the combined projectile and effective added mass, i.e. x=h, the plate thickness. At that time the entire target material forward of the projectile moves together with it at the same velocity. The force F_c therefore becomes zero at the end of the second stage. A parabolic function for $F_{c2}(x)$ that meets the limiting conditions has been used in the analysis,

$$F_{c2}(x) = \sigma_c A_2 \left\{1 - \left[\frac{x-(h-b)}{b}\right]^2\right\} \qquad h-b \le x \le h \qquad (13)$$

The alternative choices of linear functions or similar forms that represent the limiting conditions were found to have small effect on the calculated residual velocities. It is interesting to note that Eq. (13) does lead to force-time curves which are very similar to those obtained in the case of dynamic punching, e.g. Dowling, Harding and Campbell [14].

The second stage of penetration is also characterized by a shearing force. This acts along the surface of that part of the plug which is moving together with the projectile, i.e. along the surface $\pi D_2[x-(h-b)]$ where D_2 is the diameter of the cavity in the second stage. The shear force is then given by

$$F_{s2}(x) = \tau\pi D_2\,[x-(h-b)] \qquad h-b \leq x \leq h \tag{14}$$

The shear strength of metals τ has been found to have a viscous dependence on strain rate at very high rates of straining, e.g. [16], [17]. The shear strength can be taken to be in the Bingham form

$$\tau = \tau_0 + \mu\dot{\gamma} \tag{15}$$

where μ is the coefficient of viscosity and $\dot{\gamma}$ is the shear strain rate. The latter can be taken as V/e where e is the radial transition distance between the plug and the undeformed target material, i.e. the width of the shear zone The quantity e is referred to as the "radial clearance" in dynamic punching problems and it is essentially a property only of the target material at high rates of deformation and can be readily obtained experimentally. Analytical expressions for e can be deduced from the results given in [18] and [19].

The equation of motion for the second stage is the same as that derived for the earlier one with the change in the expression for the compressive force (13) and the addition of the shearing force (14), (15).

The equation then becomes, for the case of constant D_2 and A_2

$$\frac{d}{dt}(mV) = F_2 = -\frac{1}{2}K\rho A_2V^2 - (\tau_o+\mu\frac{V}{e})\pi D_2[x-(h-b)] - \sigma_c A_2\{1-[\frac{x-(h-b)}{b}]^2\} \quad (16)$$

where $h-b \leq x \leq h$. Substituting Eq. (9) into Eq. (16) leads to

$$\frac{dV_2(x)}{dx} = \Big[-(1+0.5K)\rho A_2V^2 - \tau_o\pi D_2x - \frac{\mu\pi D_2}{e}Vx + \frac{\mu\pi D_2(h-b)}{e}V + \tau_o\pi D_2(h-b) - \sigma_c A_2\{1-[\frac{x-(h-b)}{b}]^2\}\Big] \Big/ [(m_1+\rho A_2x)V] \quad (17)$$

where $m_1 = m_o+\rho A_1(h-b)$ is the effective mass at the end of the first stage.

The time t for the combined projectile and added mass to reach the rear surface of the target plate, i.e. $x=h$, is calculated by numerical integration of

$$t_2 = \int_{x=h-b}^{x=h} \frac{1}{V}\,dx \quad (18)$$

V can be calculated numerically by a computer subroutine from Eq. (17). The force time curve can be obtained from Eqs. (16), (17) and (18).

The third stage commences when the entire section of target material forward of the projectile moves together with it as a rigid body. The effective mass is then $m_2=m_o+\rho\bar{A}h$ where $\bar{A}$ is the average cross sectional area of the entire cavity. During stage 3 the only active force is that due to the shear stresses acting over the surface of the plug. These shearing stresses are considered to act in a shear zone of depth e around the plug.

The displacement, ξ, of the combined projectile and added mass system with respect to the plate is therefore related to e by

$$\xi = \gamma e \tag{19}$$

where γ is the shear strain in the effected zone. The displacement for material failure, ξ_f, is reached at the maximum shear strain of the material, γ_f, i.e. $\xi_f = \gamma_f e$, beyond which no further resisting forces act on the moving system. The shear strain that was developed in the second stage is small and could be neglected. The equation of motion for the third stage is therefore

$$m_2 \frac{d^2\xi}{dt^2} - F_3 = -\tau A_p \tag{20}$$

where $A_p = \pi D_2 b$ and D_2 is the average cavity diameter in the second stage.

Using Eq. (15) for τ, Eq. (20) becomes

$$\ddot{\xi} + \frac{A_p \mu}{m_2 e} \dot{\xi} = - \frac{\tau_o A_p}{m_2} \tag{21}$$

which can be readily solved for $\dot{\xi}$ and ξ.

$$\dot{\xi} = \left(\bar{V}_2 + \frac{\tau_o e}{\mu}\right) \left[\exp\left(- \frac{A_p \mu}{m_2 e} t\right)\right] - \frac{\tau_o e}{\mu} \tag{22}$$

$$\xi = \left(\bar{V}_2 + \frac{\tau_o e}{\mu}\right) \left(\frac{m_2 e}{\mu A_p}\right) \left[1 - \exp\left(- \frac{A_p \mu}{m_2 e} t\right)\right] - \frac{\tau_o e}{\mu} t \tag{23}$$

where $\bar{V}_2$ is the velocity at the end of the second stage. The force during this stage can therefore be expressed as

$$F_3 = -A_p\left(\tau_o + \mu \frac{\bar{V}_2}{e}\right)\left[\exp\left(-\frac{A_p\mu}{m_2 e} t\right)\right] \tag{24}$$

The time duration of the third stage t_3 is determined by the time required for the displacement ξ to reach ξ_f. The corresponding velocity at this time $\bar{V}_3$ is the final velocity of the projectile V_f. The force-time relations for this stage can then be determined from the preceding equations.

The total time for the perforation process is the sum of those of the three stages plus the time required for the plug to leave the target plate. That is

$$t_f = t_1 + t_2 + t_3 + \frac{b-\xi_f}{V_f} \tag{25}$$

It is noted that this time would correspond to that of full ejection of the plug. This would then be followed by ejection of fragments corresponding to the effective mass added during stage 1 and then by the projectile itself.

Discussion

The preceding expressions enable the post perforation velocity, force-time history, and contact time to be calculated for penetration processes that include dishing, plug formation, and ductile cavity enlargement. The relative importance of the mechanisms considered in the analysis would be determined by the various physical, mechanical, and geometrical parameters appearing in the equations. Of these, a few have to be determined empirically, namely the entrance and exit hole diameters D_1 and D_3 and the plug length b. Values for the coefficient of viscosity μ and the width of the shear zone e can be obtained from the results of other investigations and modified to suit the particular ballistic test conditions.

The geometrical measurements to be taken on experimental target plates are D_1, D_3 and b. Fairly good results can be obtained by simply setting $D_2 = D_{avg} = 1/2\ (D_1+D_3)$ and setting $A_1 \approx A_2$ for the area corresponding to D_{avg}. For cases where $D_3 >> D_1$, it would be more exact to calculate A_1 on the basis of D_1, and to take D_2, which is the average diameter of the plug, to be the linear average of D_1 and D_3 over the plug distance b. A large number of measurements on a variety of perforated plates [10], [15] has shown that the ratios D_{avg}/h, and b/h are essentially constant for a given target plate material and projectile over the range of velocities of interest. This means that those parameters could be obtained from relatively few tests and then used in the equations to obtain results for other test conditions.

The viscosity of materials at high shearing rates has been determined by various rapid loading experiments, e.g. [14], [16], and [17]. These results could be used for μ in the analysis. The perforation process itself is a rapid loading experiment so μ could be considered an experimentally determined material property within the framework of the analysis. That is, μ for a given plate material could be set so that the computed results would best fit the test results. In practice, the values of μ deduced from the ballistic tests and those that had been obtained from more direct measurements are generally in good agreement [15].

The width of the shear zone, e, could be obtained experimentally by examination of etched specimens or can be deduced from the analyses of [18] and [19]. Again both methods seemed to be in reasonable agreement. Either could be used since the results are not sensitive to the exact value of e.

The dependence of the residual velocity on the properties of the projectile and target plate and on the test conditions appear to be in conformity with general observations on projectile perforation. A typical set of force-time, velocity-time, and displacement-time diagrams obtained from the analysis is shown in Fig. 2. This example was calculated for the case of a 0.22 inch caliber lead bullet perforating a 5.0 mm thick aluminum alloy plate. The component forces throughout the three stages are shown in Fig. 3 for the same case.

The absence of an initial rise time for the force is due to the neglect of the shape of the nose of the projectile on the rise time of action of the compressive and inertial forces. Those forces are assumed to act immediately on the full cross section. Consideration of this effect would have only a

very small influence on the overall results. The decay of the total force during the first stage is due to the decrease of the inertial force. The shear force acting in the second and third stages is seen to be important and dominant in the last part of the perforation process. A discontinuity in the force (dotted lines in Figs. 2&3) would appear at the onset of the third stage due to the removal of the inertial force. Force continuity could be maintained by suitably changing the value of e, the width of the shear zone. Detailed examination of ejected plugs has indicated that corresponding changes in e do, in fact, take place during the ejection stage. The alteration of e in the analysis to ensure force continuity therefore seems to have a physical basis.

A comparison of the predicted force-time relations with those obtained in dynamic punching experiments, e.g. Fig. 4 from [14], shows reasonable agreement. In those curves, the time over which the force decreases after the first peak would correspond to stage 1, i.e. before the onset of plugging.

There are important differences between the force-time histories obtained from the present analysis and those obtained in [11] on the basis of an assumed deceleration-time function of the projectile. In [11] the force tends to zero in the last part of the process while the present results indicate that the final force is still close to its maximum value.

There are experimental indications that the force is large at the last stage of perforation. This is the observation made in [11] and other ballistic experiments that the velocity drop i.e. the difference between initial and final velocities, diminishes for velocities slightly in excess of the ballistic limit, e.g. Fig. 21 of [11]. This result corresponds to the obser-

vation that a projectile that perforates a plate under conditions slightly exceeding the ballistic limit, i.e. a higher initial velocity or thinner target plate, would have a relatively high terminal velocity, e.g. about 20% of the initial value. The impulse associated with the end process of perforation is therefore significant. This in turn implies that the force acting during the end process is high which is in accordance with the results shown in Figs. 2 and 3. Another consideration is that the time interval for the third stage, t_3, is found to be sensitive near the ballistic limit, and small increases in thickness or decreases of velocity would increase t_3 by a relatively large amount. This effect and a large terminal force are the apparent causes of the observations on the velocity drop effect. The predictions of terminal velocities based on the present analysis [15] do, in fact, show that the velocity drop initially decreases with increasing initial velocity as indicated in Fig. 21 of [11].

Conclusions

The analysis of the ballistic perforation problem that has been developed seems capable of predicting post perforation velocities, contact times, and force-time histories. The analysis relies on certain geometrical parameters which must be determined empirically at this stage of development. Certain material properties are not well established and could be determined by extrapolation of other results or by experimental observations. Both these and the empirical geometrical parameters could be obtained from a small number of tests. Once these are determined for a given projectile and target material, predictions can be obtained over a wide range of projectile velocities and target thicknesses. Further development of the analysis would be to determine the empirical factors by basic considerations.

References

1. W. Goldsmith, Impact; The Theory and Physical Behaviour of Colliding Solids. Edward Arnold, Ltd., London (1960).

2. G.I. Taylor, The formation and enlargement of a circular hole in a thin plastic sheet. Quart. J. Mech. Appl. Math. vol. 1, 103-124 (1948).

3. W.T. Thomson, An approximate theory of armor penetration. J. Appl. Phys. vol. 26, 80-82 (1955).

4. A. Brown, A quasi-dynamic theory of containment. Int. J. Mech. Sci., vol. 6, 257-262 (1964).

5. M. Zaid and B. Paul, Mechanics of high speed projectile perforation. J. Franklin Inst., vol. 264, 117-126 (1957).

6. B. Paul and M. Zaid, Normal perforation of a thin plate by truncated projectiles. J. Franklin Inst., vol. 265, 317-335 (1958).

7. J. Nishiwaki, Resistance to the penetration of a bullet through an aluminum plate. J. Phys. Soc., Japan, vol. 6, 374-378 (1951).

8. R.F. Recht and T.W. Ipson, Ballistic perforation dynamics. J. Appl. Mech., vol. 30, 384-390 (1963).

9. W. Goldsmith, T.W. Liu and S. Chulay, Plate impact and perforation by projectiles. Experimental Mechanics, vol. 5, 385-404 (1965).

10. J. Awerbuch, A mechanics approach to projectile penetration. Israel J. of Tech., vol. 8, 375-383 (1970).

11. W. Goldsmith and S.A. Finnegan, Penetration and perforation processes in metal targets at and above ballistic velocities. Int. J. Mech. Sci., vol. 13, 843-866 (1971).

12. J.M. Krafft, Surface friction in ballistic penetration. J. Appl. Phys., vol. 26, 1248-1253 (1955).

13. R.M. Davies, Stress Waves in Solids, Surveys in Mechanics, edited by G.K. Batchelor and R.M. Davies, Cambridge University Press, 64-139 (1956).

14. A.R. Dowling, J. Harding and J.D. Campbell, The dynamic punching of metals. J. Inst. Metals, vol. 98, 215-224 (1970).

References (cont'd)

15. J. Awerbuch and S.R. Bodner, Experiments on the normal perforation of projectiles in metallic plates, MED Report No. 41, June 1973, Dept. of Materials Engineering, Technion, Haifa, Israel.

16. W.G. Ferguson, A. Kumar and J.E. Dorn, Dislocation damping in aluminum at high strain rates. J. Appl. Phys., vol. 38, 1863-1869 (1967).

17. J.D. Campbell and W.G. Ferguson, The temperature and strain-rate dependence of the shear strength of mild steel. Phil. Mag., vol. 21, 63-82 (1970).

18. P.C. Chou, Perforation of Plates by High Speed Projectiles, Developments in Mechanics, edited by J.E. Lay and L.E. Malvern, North-Holland Publishing Co., Amsterdam, vol. 1, 286-295 (1961).

19. R.G. Thomson, Analysis of hypervelocity perforation of a visco-plastic solid including the effects of target-material yield strength. NASA TR R-221 (1965).

List of Captions

Fig. 1 - Schematics of the stages of the perforation process.

Fig. 2 - Calculated example of displacement, velocity, and force histories for the three stages of perforation.

Fig. 3 - Force-time relation for each of the force components for the three stages of perforation (same conditions as Fig. 2).

Fig. 4 - Load/Displacement curves for aluminum (from Ref. [14]).

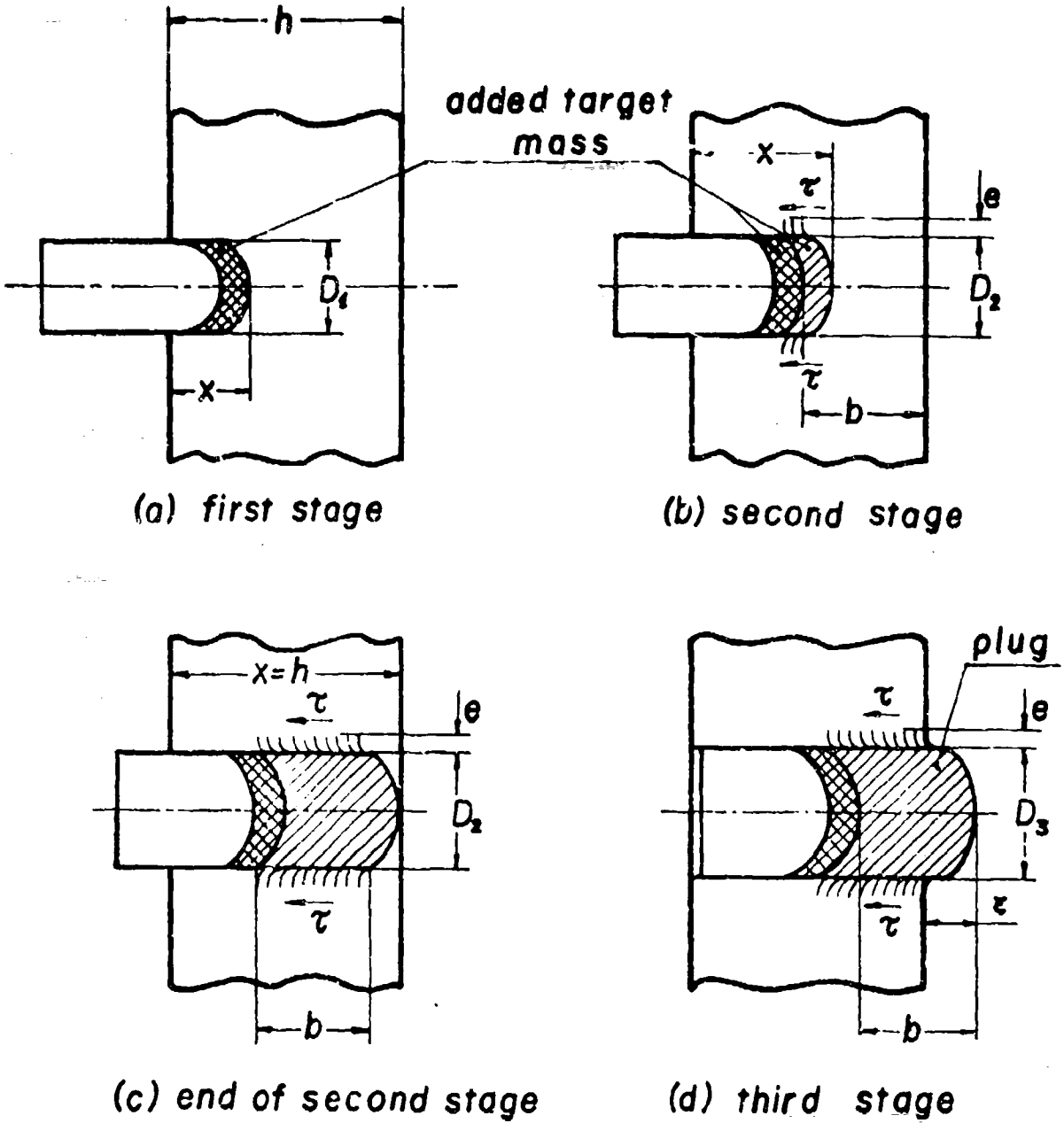
h
added target mass
x
τ
e
D_1
D_2
τ
b
(a) first stage
(b) second stage
x=h
τ
e
D_2
τ
b
plug
τ
e
D_3
τ
τ
b
(c) end of second stage
(d) third stage

Fig. 1

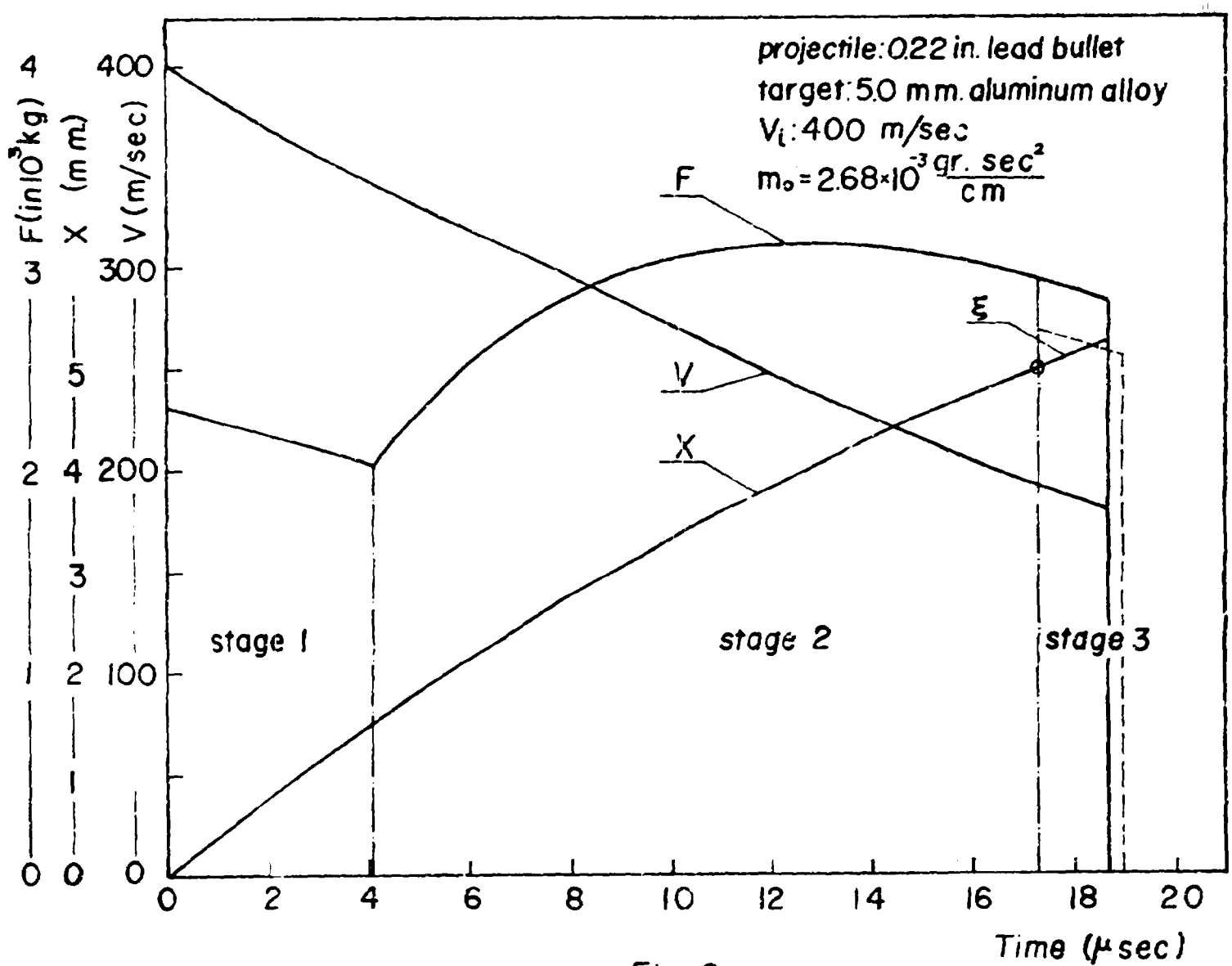
projectile: 0.22 in. lead bullet
target: 5.0 mm. aluminum alloy
V_i: 400 m/sec
$m_o = 2.68 \times 10^{-3} \frac{gr.\ sec^2}{cm}$
F
V
X
ξ
stage 1
stage 2
stage 3
F (in 10^3 kg)
X (mm)
V (m/sec)
Time (μsec)
0
1
2
3
4
0
2
4
6
8
10
12
14
16
18
20
0
100
200
300
400
0
1
2
3
4
5

Fig. 2

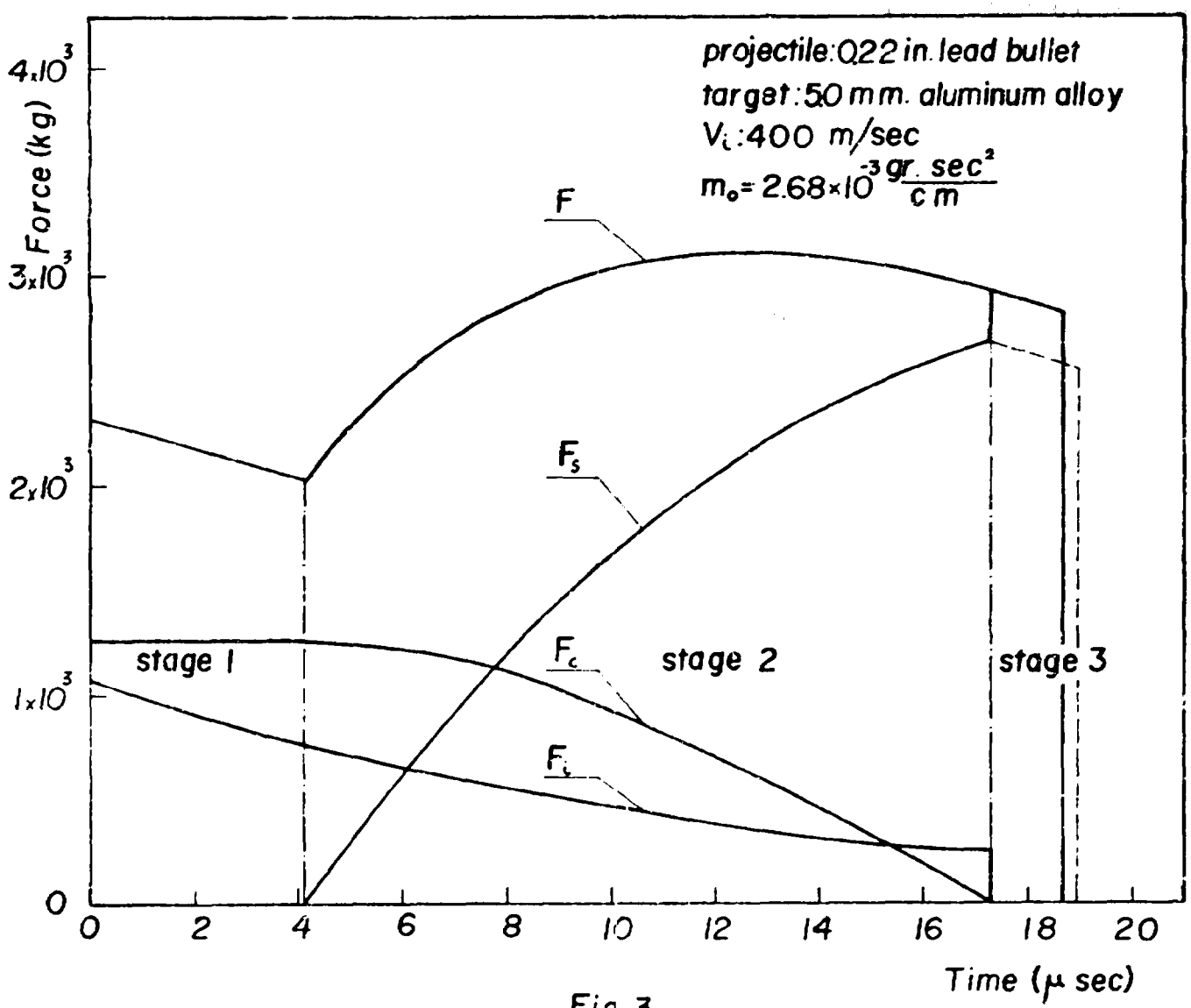
projectile: 0.22 in. lead bullet
target: 5.0 mm. aluminum alloy
V_i: 400 m/sec
$m_o = 2.68 \times 10^{-3} \frac{gr.\ sec^2}{cm}$
F
F_s
F_c
F_i
stage 1
stage 2
stage 3
Force (kg)
4×10^3
3×10^3
2×10^3
1×10^3
0
0
2
4
6
8
10
12
14
16
18
20
Time (μ sec)

Fig. 3

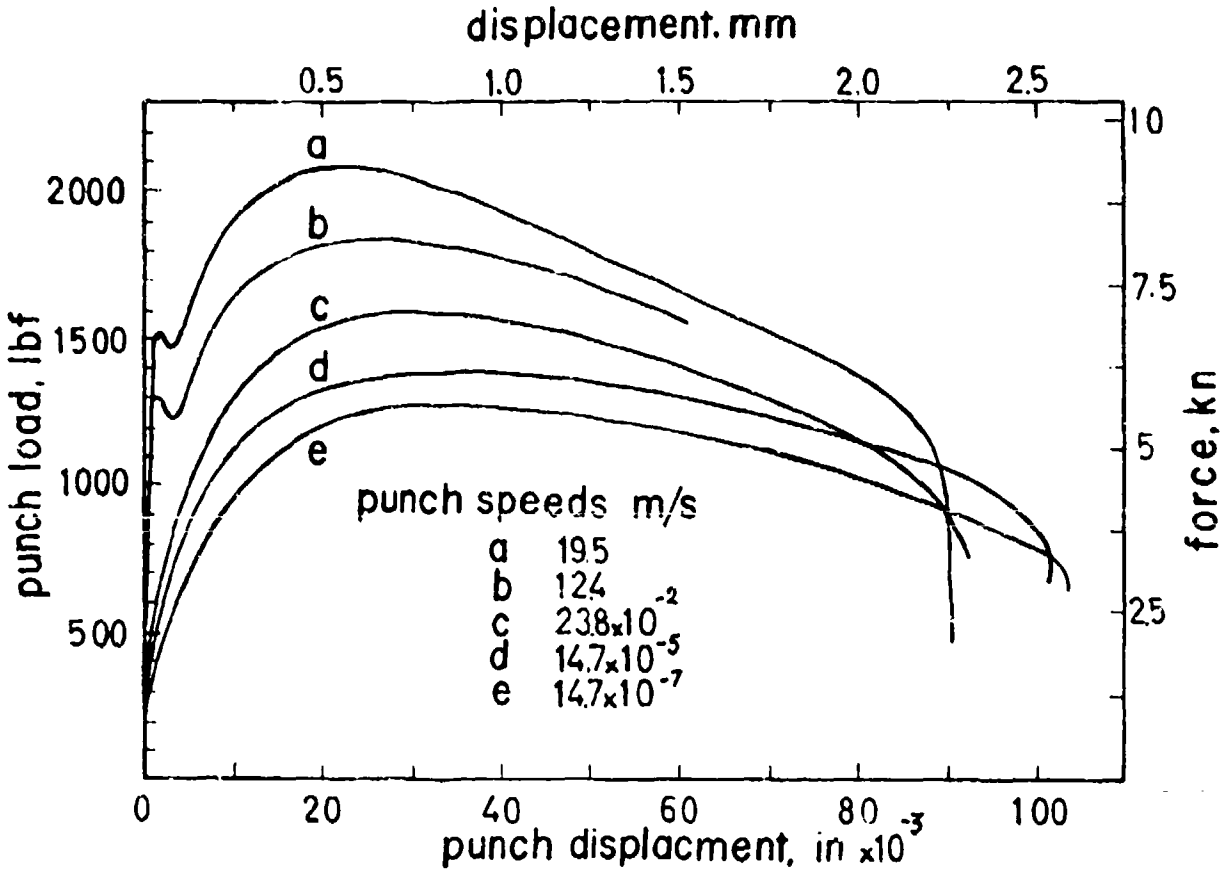
displacement. mm
0.5
1.0
1.5
2.0
2.5
punch load, lbf
2000
1500
1000
500
force, kn
10
7.5
5
2.5
a
b
c
d
e
punch speeds m/s
a 19.5
b 12.4
c 23.8x10^-2
d 14.7x10^-5
e 14.7x10^-7
0
20
40
60
80
100
punch displacment, in x10^-3

Fig. 4